

Military Technical College  
Kobry Elkobbah,  
Cairo, Egypt



8<sup>th</sup> International Conference on  
Aerospace Sciences &  
Aviation Technology

## TRAJECTORY SIMULATION OF OGIVAL-BOAT-TAILED PROJECTILES

A. Zaki\*, M.S. Abdel-Kader\*\*, and H. Yakout\*\*\*

### ABSTRACT

Resistance to projectile flight in air decomposes into three main components. The first component is the nose drag due to the air pressure ahead of the body. The second is the skin friction drag component due to shear forces between the air layers. The third is the total base drag component due to disability of air stream lines to follow up the body shape specially at supersonic speeds. Herein, it is shown how different drag coefficients, and consequently total drag coefficient, can be predicted.

Drag models can be empirical or semi-empirical. A combination of two drag models will be used herein in order to predict drag coefficients at Mach numbers ranging from 0 to 3.5 for different projectile shapes. These models are the semi-empirical model introduced by Lebeqev and Chernobrovsky and the experimental data illustrated graphically by ESDU.

Drag prediction of classical and modern projectile shapes with boat-tails is conducted for different initial firing conditions. Effect of changing projectile shape on range is discussed. It is concluded that the range is increased in case of projectiles having longer ogive and boat-tail, and boat-tail angle ranging from 3 to 5 degrees.

### KEY WORDS

Trajectory Simulation, Drag Modeling, Ogival Boat-Tailed Projectiles.

### INTRODUCTION

During projectile flight in air, the total drag coefficient decomposes into three parts, that is:

$$C_D(M, Re) = C_{DN}(M) + C_{DSF}(M, Re) + C_{DA}(M), \quad (1)$$

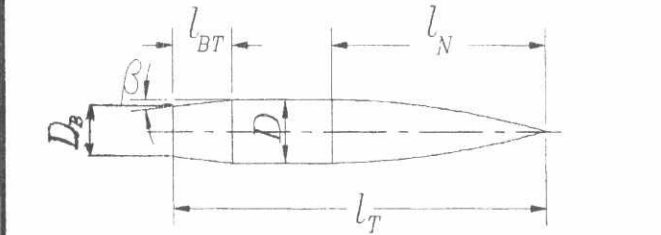
where  $C_{DN}$ ,  $C_{DSF}$  and  $C_{DA}$  are the nose, viscous, and afterbody drag coefficients, respectively. Assuming axi-symmetric, ogival boat-tailed projectile, the afterbody drag divides into the base pressure drag  $C_{DBP}$  and the boat-tail drag  $C_{DBT}$ , that is:

\* Assistant Lecturer, \*\* Associate Prof., and \*\*\* Lecturer, Department of Aerospace Engineering, M.T.C., Cairo, Egypt.

$$C_{DA}(M) = C_{DBP}(M) + C_{DBT}(M), \tag{2}$$

A number of drag models have been introduced to predict drag coefficients, [1-6]. In a previous study [7], it was concluded that for ogival boat-tailed projectiles, the semi-empirical model of Lebeqev and Chernobrovsky [5] gives good results for  $C_{DN}$  and  $C_{DSF}$ . On the other hand, the afterbody drag coefficient  $C_{DA}$  is best predicted using the experimental data of Refs. [2-4]. In the following sections, component and total drag coefficients will be predicted for different projectile dimensions within the limits listed in Table (1).

Table 1 Limits of projectile dimensions



Nose length	$l_N$	(2-5) D
Base diameter ratio	$D_B/D$	0.6-1.0
Boat-tail angle	$\beta$	3°-10°

**NOSE AND SKIN FRICTION DRAG MODELING**

According to Ref. [5], the nose drag coefficient can be obtained as function of Mach number and nose length. Moreover, the skin friction drag coefficient is calculated from:

$$C_{DSF} = \frac{1}{2} C_{f_0} E_M K_{CN} \frac{A_T}{A}, \tag{3}$$

where  $C_{f_0}$  is the flat plate skin friction coefficient at zero Mach number.  $C_{f_0}$  is a function of Reynolds number (Re) and the normalized laminar boundary layer length ( $\bar{X}_t$ ), which is equal to the ratio of the laminar boundary layer to the projectile total length.

Similarly, the function  $E_M$  introduces the effect of Mach number for a certain boundary layer length. Moreover, the function  $K_{CN}$  accounts for the effect of projectile front shape and changes with ogive length and Mach number.

In Eq. (3),  $A (= \pi D^2/4)$  and  $A_T$  are the maximum cross section area of the projectile and the total wetted area of the projectile surface, respectively.

It is assumed that the front of the projectile is conical in shape ( $\bar{X}_t=0.0$ ) and the characteristic length is the projectile ogive length. The rear part (cylinder and boat-tail) of the projectile is considered to be cylindrical, that is ( $\bar{X}_t=0.0$  and function  $K_{CN}=1$ ). Also, the characteristic length is the summation of both cylinder and boat-tail lengths. Thus, the final equation which is applied to get  $C_{DSF}$  will have the following form:

$$C_{DSF} = \frac{1}{2} \left( C_{fo} E_M K_{CN} \frac{A_T}{A} \right)_{ogive} + \frac{1}{2} \left( C_{fo} E_M \frac{A_T}{A} \right)_{cyl.+boat-tail} \quad (4)$$

### AFTERBODY DRAG MODELING

The afterbody drag components (cf. Eq. (2)) were estimated through wind tunnel tests in the three main regions of Mach number. (subsonic, transonic and supersonic) by ESDU [2-4]. In the following subsections, the base pressure drag and boat-tail drag coefficients will be predicted for different afterbody dimensions and Mach numbers ranging from 0.0 to 3.5.

#### 1. Base Pressure and Boat-Tail Drag in Subsonic Speed Region

According to Ref. [2], the base pressure drag is obtained as function of base diameter ratio ( $D_B/D$ ) and boat-tail angle ( $\beta$ ), as shown in Fig. (1). Note that negative values of base pressure drag can be obtained, which will be compensated by summing the corresponding values of boat-tail drag coefficient. The latter coefficient in this speed region is predicted from graphs illustrated in carpet form [2].

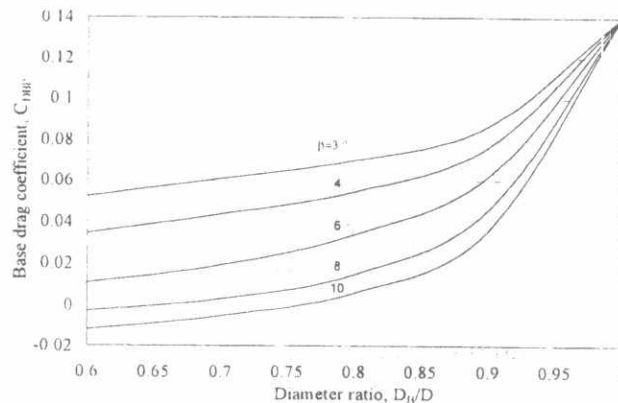


Fig. 1 Base drag coefficient for  $M \leq 0.8$  [2]

#### 2. Base Pressure and Boat-Tail Drag in Transonic Speed Region

$C_{DBP}$  and  $C_{DBT}$  were predicted using a family of curves in the carpet form at different Mach numbers [3]. Note that these data are based on the assumption that the flow remains fully attached to the projectile boat-tail surface.

#### 3. Base Pressure and Boat-Tail Drag in Supersonic Speed Region

Similarly,  $C_{DBP}$  was predicted, at different Mach numbers, using curves issued by ESDU [4]. On the other hand, boat-tail drag coefficient in this speed region is estimated by applying the following empirical formula, which is a modification of Kransov empirical equation [8]:

$$C_{DBT} = C(\beta, D_B/D) \left( 0.08 + \frac{1}{M^2} \right) \beta^{1.7} \frac{A_B}{A} \quad (5)$$

where  $C$  is a coefficient which varies with the projectile afterbody dimensions ( $\beta$ ,  $D_B/D$ ), as shown in Fig. (2).

### PREDICTION OF TOTAL DRAG COEFFICIENT

Referring to Eq. (1), the total drag coefficient of an ogival boat-tailed projectile is predicted by the sum of the nose, base, boat-tail and viscous drag coefficients. The data of drag coefficients presented and discussed in the previous sections

These dimensions are entered to a code which estimates each of the drag coefficients and plots them with Mach number. It was assumed that there is no meteorological effect and the projectile is at zero incidence angle with the air flow.

Table (2) Dimensions of projectile P1 relative to P2

Caliber ( $D_1/D_2$ )	1.00
Total Length ( $L_{T1}/L_{T2}$ )	1.08
Nose Length ( $L_{N1}/L_{N2}$ )	1.14
Boat-Tail Length ( $L_{BT1}/L_{BT2}$ )	3.30
Boat-Tail Angle ( $\beta_1/\beta_2$ )	0.47

In the subsequent analysis two projectiles are considered, which will be referred to as P1 and P2, respectively (cf. Table (2)). Figure (3) shows the change of each of the drag components with Mach number.

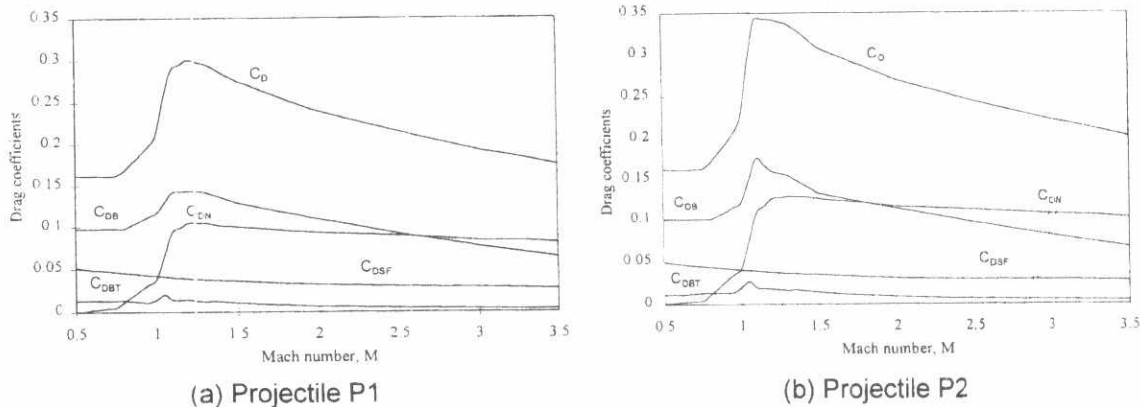


Fig. 3 Drag coefficients versus Mach number

**TRAJECTORY SIMULATION**

The analysis is based on the following assumptions: (i) the projectile is considered to be a point mass moving with two degrees of freedom (x-y plane), (ii) the air resistance force is collinear with projectile axis, and (iii) the air resistance force consists of the main drag components (nose drag, viscous drag and total base drag forces).

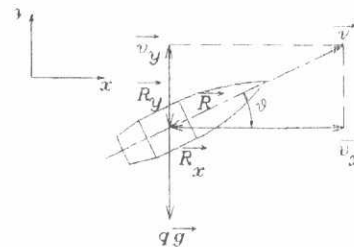


Fig.4 Forces acting on the projectile during flight

Figure (4) shows the forces acting on a typical projectile during flight. Applying Newton's second law, the projectile equations of motion in the x and y directions will be:

$$q \frac{dv_x}{dt} = -R \cos\theta, \quad q \frac{dv_y}{dt} = -R \sin\theta - qg, \tag{6}$$

where  $v_x$  and  $v_y$  are the components of projectile velocity in both x and y directions,  $t$  is the instantaneous time of flight,  $R$  is the total air resistance force,  $q$  is the projectile mass and  $g$  is the gravitational acceleration. The air resistance force is given by the following equation:

$$R = \frac{1}{2} \rho_\infty v^2 S C_D(M, Re). \tag{7}$$

The upstream air density  $\rho_\infty$  is assumed to change with the projectile altitude according to the following equations [9]:

$$\rho_\infty = 1.225 \left( 1 - 0.0065 \frac{y}{T_0} \right)^{4.256}, \quad (0 \leq y \leq 11000 \text{ m}),$$

$$\rho_\infty = \rho_{11000} \cdot e^{1.57 \cdot 10^{-4} (11000 - y)}, \quad (y > 11000 \text{ m}),$$
(8)

where  $y$  is the projectile height,  $T_0$  is the air temperature at sea level, and  $\rho_{11000}$  is the air density at 11000 m height. The differential equations of the projectile velocity in both  $x$  and  $y$  directions will be:

$$v_x = \frac{dx}{dt}, \quad v_y = \frac{dy}{dt}.$$
(9)

To solve Eqs. (6) and (9),  $C_D(M)$  must be known at every point. Consequently, Mach and Reynolds numbers must be estimated. The latter number is given by [9]:

$$Re = \frac{\rho_\infty v L_T}{\mu},$$
(10)

$$\mu = \mu_0 \left( \frac{T}{T_0} \right)^{1.5} \frac{(T + 110)}{(T_0 + 110)},$$
(11)

where  $L_T$  is the projectile total length,  $\mu$  is the air viscosity and  $\mu_0$  is the viscosity at sea level ( $\mu_0 = 1.789 \times 10^{-5} \text{ N.s/m}^2$ ). Moreover, the following equations relate air temperature in Kelvin to projectile altitude:

$$T = T_0 - 0.0065 y, \quad (0 \leq y \leq 11000 \text{ m}),$$

$$T = 217, \quad (y > 11000 \text{ m}).$$
(12)

Thus, by solving the system of the differential equations (6), (9) numerically, the projectile trajectory parameters can be estimated.

Applying the chosen drag model on the projectiles P1 and P2, the trajectory parameters were predicted at standard firing conditions. The errors in maximum ranges were found to be 0.3 % and 2.7%, respectively, with reference to the tabulated values. These trajectories are shown in Fig. (5) in normalized forms.

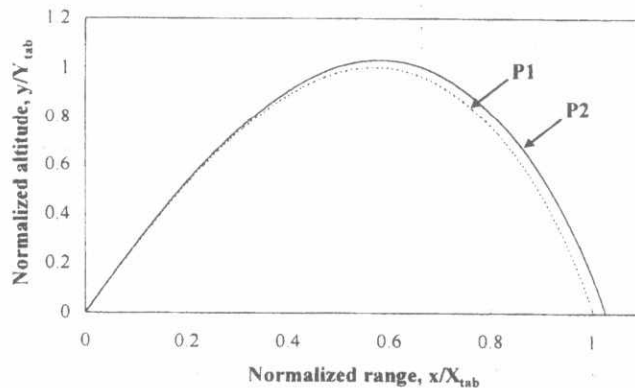


Fig. 5 Normalized trajectories of projectiles P1 and P2

RESULTS AND DISCUSSIONS

The potential of the drag model presented herein will be checked via comparing the drag curves it predicts with those of PRODAS software [11] as well as with real measurements. The initial conditions of these measurements were recorded. Then, the range and side deviation were measured. The projectiles were also tracked by the radar and the instantaneous trajectory parameters at any point on the trajectory were determined.

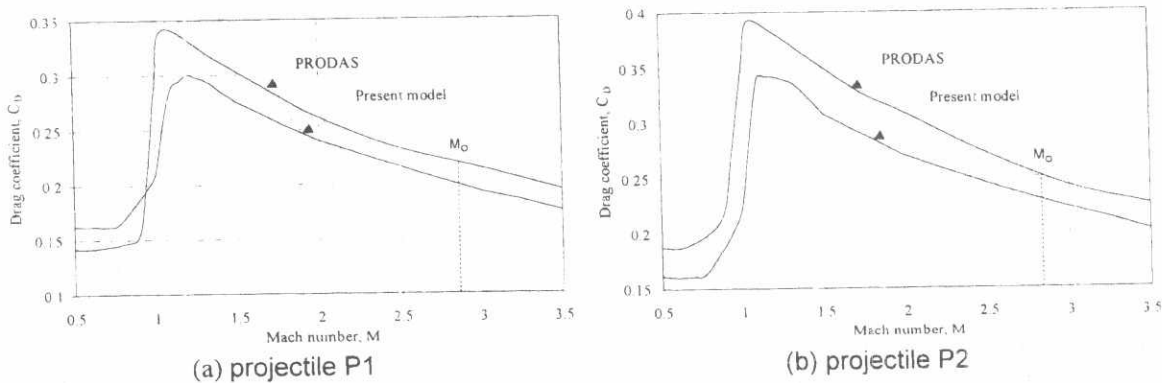


Fig. 6 Predicted drag coefficient versus Mach number

Figure (6) illustrates the drag coefficients of the projectiles P1 and P2. This figure shows the difference between the prediction of the present model and that of PRODAS. In general, it is clear that the model used herein predicts lower values of drag than those predicted by PRODAS. Past experience with PRODAS indicates that it normally overestimates drag. That is why a drag form factor, which is lower than unity, is recommended in this software.

Figure (7) illustrates the total drag coefficients measured using the tracking radar and their counterparts predicted using the present model for the projectile P2 at different initial firing conditions. It is clear that the predicted values of the drag coefficient are generally higher than those measured in supersonic speed region. On the contrary,  $C_D(M)$  is inverted at transonic speeds.

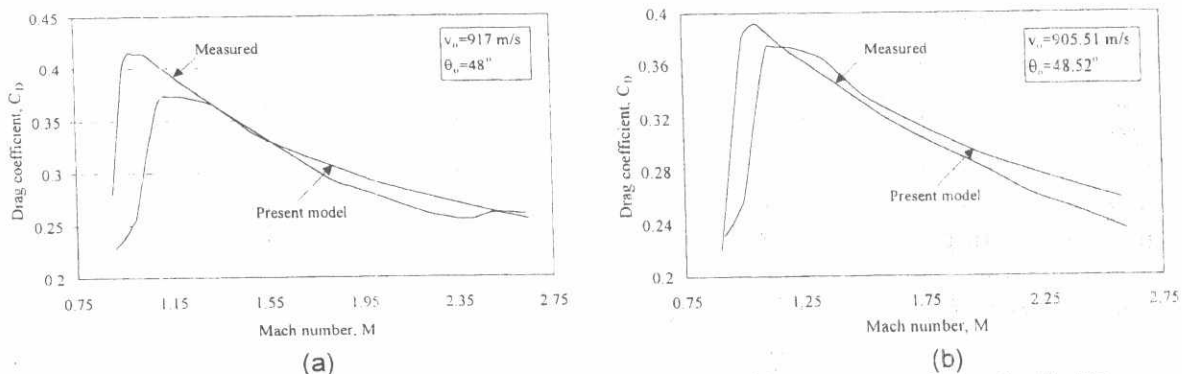


Fig. 7 Predicted and measured drag coefficient versus Mach number for projectile P2

Further comparisons between the model output and real firing data were made, and good agreement was generally obtained; in terms of maximum range, an accuracy of less than 2.7% was ascertained.

Having validated the model, it is now shown how to use it to find the optimum shape (afterbody dimensions and ogive length) that maximizes the range. The afterbody shape depends on the boat-tail length ( $L_{BT}$ ) and angle ( $\beta$ ). Figure (8) illustrates the change in range due to variation of boat-tail length for boat-tail angles ranging from  $3^\circ$  to  $10^\circ$ . It is obvious that the increase of boat-tail angle is recommended especially at high boat-tail length, but the stability is affected diversely.

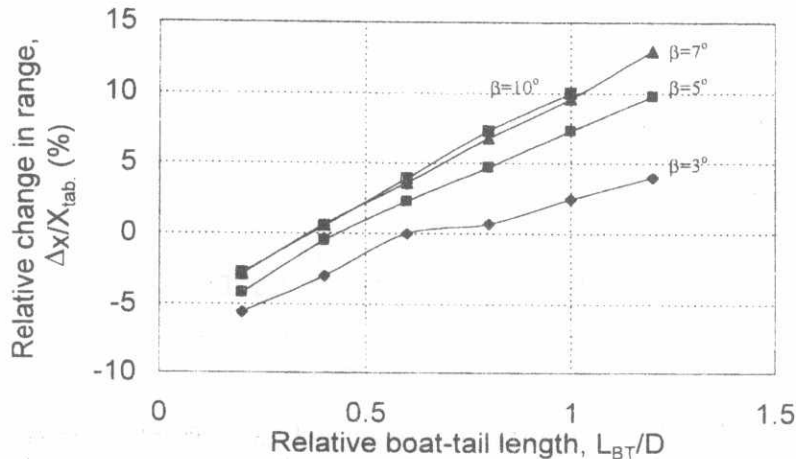


Fig. 8 Percentage increase in range with boat-tail length and angle

The optimum boat-tail length of the projectile P1 is equal to  $0.8 D$ , because at this value the projectile stability on trajectory is well achieved. The stability of any spinning projectile depends on two main factors; the first is the gyroscopic stability factor,  $S_g$ , which represents the stability of the projectile at the moment of muzzle exit and the second is the dynamic stability factor,  $S_d$ , which represents the regularity of projectile flight i.e. the change of yaw with elevation at the ascendant arc of the trajectory [10].

Figure (9) illustrates the relationship between  $S_d$  and  $1/S_g$  determined by PRODAS [11]. The crossmarks on this graph correspond to the values of  $S_d$  and  $1/S_g$  at specified Mach numbers (from left to right  $M=0.95$  to  $3.0$ ). For the projectile to be dynamically and gyroscopically stable, the crossmarks should lie below the parabola having the equation:

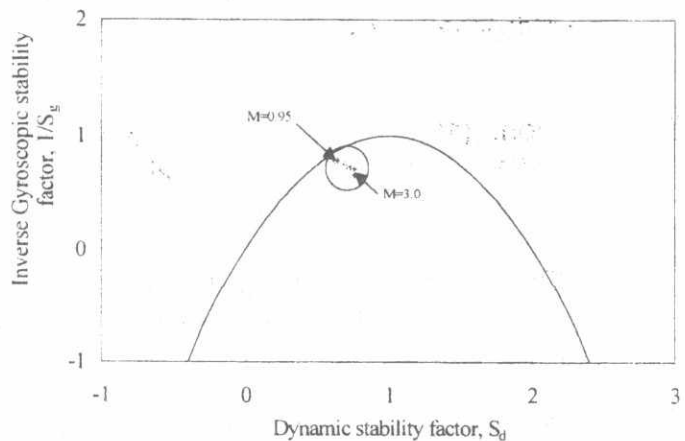


Fig.9 Dynamic stability criteria

$$\frac{1}{S_g} = S_d(2 - S_d) \tag{13}$$

to get the maximum range and, at the same time, keep the projectiles stable on trajectory, the optimum boat-tail angle and length should be 5° and 0.8D, respectively. These values represent the coordinates of point A in Fig. (10).

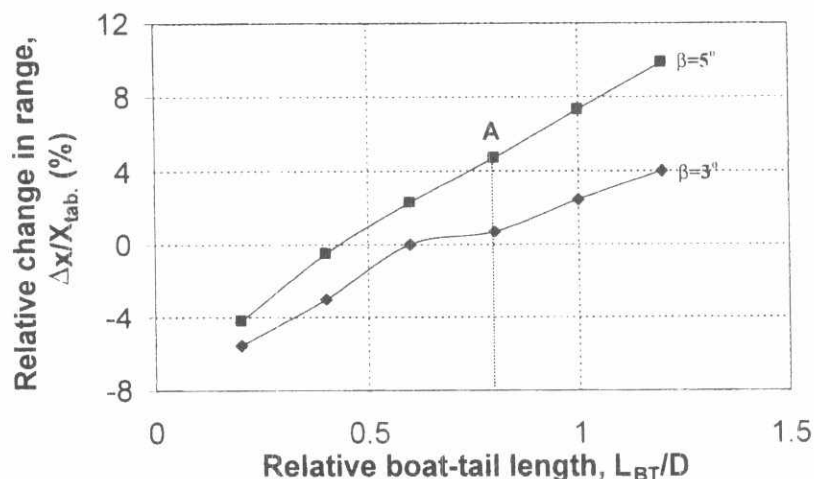


Fig. 10 Percentage increase in range with boat-tail length and angle

To conclude, the afterbody dimensions (boat-tail angle and length) affect the projectile range; the optimum boat-tail angle ranges from 3° to 5° and the boat-tail length from 0.75D to 1.0D. Also, the drag on the projectile decreases with the increase of the ogive length, but this increase affects the projectile stability during its motion on trajectory diversely.

REFERENCES

- [1] Anon. (1963), "External Ballistics: Part I," Military Technical College Printed Lectures, No. 208, Cairo.
- [2] Anon. (1976) "Subsonic Base Drag of Cylindrical Bodies with Conical Boat-tails," Report No. ESDU-76033, Engineering Science Data Units Ltd., London.
- [3] Anon. (1978) "Transonic Base and Boat-tail Pressure Drag of Cylindrical Bodies with Conical Boat-tails," Report No. ESDU-78041, Engineering Science Data Units Ltd., London.
- [4] Anon. (1979) "Supersonic Base Drag of Cylindrical Bodies with Conical Boat-tails," Report No. ESDU-79022, Engineering Science Data Units Ltd., London.
- [5] Lebeqev A. A. and Chernobrovsky, L. S. (1973), "Flight Dynamics," Mir Publishers, Moscow.
- [6] Gany, A. (1988), "Analysis of Gun-Launched Solid Fuel Ramjet Projectiles," First International Symposium on Special Topics in Chemical Propulsion, K. K. Kenneth and J. N. Fleming, Hemisphere Publisher Corp., New York, pp. 289-309.

- [7] Karam, S. (1994) "Computer Simulation of Extended-Range Artillery Projectiles Via Base Bleeding," M. Sc. Thesis, M.T.C., Cairo, Egypt.
- [8] Kransov, N.F (1970), "Aerodynamics of Bodies of Revolution," Elsevier Publishing Company, New York.
- [9] Nelson, R.C. (1987), "Flight Stability and Automatic Control," McGraw-Hill Book Company, New York.
- [10] Smith, D.S. et al. (1966), " Design for Control of Projectile Flight Characteristics," United States Army Material Command, AMC pamphlet number 706-242.
- [11] Anon. (1993), "PRODAS Software," Arrow Tech Associates, USA.